

## **Myosin-1C augments secretion of von Willebrand factor by linking contractile actomyosin machinery to the plasma membrane**

Tracking no: ADV-2024-012590R2

Sammy El-Mansi (Queen Mary University of London, United Kingdom) Tom Mitchell (Queen Mary University of London, United Kingdom) Golzar Mobyen (Imperial College London, United Kingdom) Thomas McKinnon (Imperial College London, United Kingdom) Pika Miklavc (University of Salford, United Kingdom) Manfred Frick (Ulm University, Germany) Thomas Nightingale (Queen Mary University of London, United Kingdom)

### **Abstract:**

Blood endothelial cells control the hemostatic and inflammatory response by secreting von Willebrand factor (VWF) and P-selectin from storage organelles called Weibel-Palade bodies (WPB). Actin-associated motor proteins regulate this secretory pathway at multiple points. Prior to fusion, myosin Va forms a complex that anchors WPBs to peripheral actin structures allowing maturation of content. Post-fusion, an actomyosin ring/coat is recruited and compresses the WPB to forcibly expel the largest VWF multimers. Here we provide the first evidence for the involvement of class I myosins during regulated VWF secretion. We show that the unconventional myosin-1C (Myo1c) is recruited post-fusion via its pleckstrin homology domain in an actin-independent process. This provides a link between the actin ring and phosphatidylinositol 4,5-bisphosphate (PIP2) at the membrane of the fused organelle and is necessary to ensure maximal VWF secretion. This is an active process requiring Myo1c ATPase activity as inhibition of class I myosins using the inhibitor Pentachloropseudilin or expression of an ATPase deficient Myo1c rigor mutant perturbs the expulsion of VWF and alters the kinetics of the exocytic actin ring. These data offer a novel insight into the control of an essential physiological process and provide a new way in which it can be regulated.

**Conflict of interest:** No COI declared

**COI notes:**

**Preprint server:** Yes; bioRxiv <https://doi.org/10.1101/2023.08.11.552954>

**Author contributions and disclosures:** S.E.-M., and T.D.N., developed the methodology; P.M. and M.F. generated and provided essential tools and reagents; S.E.-M., T.D.N., T.P.M., T.A.J.M and G.M performed the investigation; T.D.N. supervised the study; S.E.-M. and T.D.N. wrote the original draft; and all authors reviewed and edited the manuscript.

**Non-author contributions and disclosures:** No;

**Agreement to Share Publication-Related Data and Data Sharing Statement:** Mass Spectrometry data is available via the PRIDE40 partner repository with the dataset identifier PXD036983 and 10.6019/PXD036983. For other original data and constructs, please contact t.nightingale@qmul.ac.uk

**Clinical trial registration information (if any):**

1 **TITLE**

2 *Myosin-1C augments endothelial secretion of von Willebrand factor by linking contractile*  
3 *actomyosin machinery to the plasma membrane*

4  
5 **SHORT TITLE**

6 *Myosin-1C augments endothelial secretion of VWF*

7  
8 **AUTHORS**

9 Sammy El-Mansi<sup>1†</sup>, Tom P. Mitchell<sup>1</sup>, Golzar Mobayen<sup>2</sup>, Thomas A. J. McKinnon<sup>2</sup>,  
10 Pika Miklavc<sup>3</sup>, Manfred Frick<sup>4</sup>, Thomas D. Nightingale<sup>1†</sup>

11  
12 **AFFILIATIONS**

13 1. Centre for Microvascular Research, William Harvey Research Institute, Barts and  
14 the London School of Medicine and Dentistry, Queen Mary University of London,  
15 London EC1M 6BQ, UK.

16 2. Department of Immunology and Inflammation, Centre for Haematology, Imperial  
17 College London, Hammersmith Hospital Campus, London, United Kingdom

18 3. School of Science, Engineering & Environment, University of Salford, Manchester  
19 M5 4WT, UK.

20 4. Institute of General Physiology, Ulm University, Albert-Einstein-Allee 11, 89081  
21 Ulm, Germany.

22  
23 † Corresponding authors: [s.elmansi@qmul.ac.uk](mailto:s.elmansi@qmul.ac.uk) and [t.nightingale@qmul.ac.uk](mailto:t.nightingale@qmul.ac.uk)

24  
25 **Correspondence**

26 Sammy El-Mansi and Thomas D. Nightingale, Centre for Microvascular Research, William  
27 Harvey Research Institute, Charterhouse Square, Faculty of Medicine and Dentistry, Queen  
28 Mary University of London, London EC1M 6BQ, United Kingdom; e-mail:  
29 [s.elmansi@qmul.ac.uk](mailto:s.elmansi@qmul.ac.uk) and [t.nightingale@qmul.ac.uk](mailto:t.nightingale@qmul.ac.uk).

30  
31 Mass Spectrometry data is available via the PRIDE40 partner repository with the dataset  
32 identifier PXD036983 and 10.6019/PXD036983. For other original data and constructs,  
33 please contact [t.nightingale@qmul.ac.uk](mailto:t.nightingale@qmul.ac.uk)

34  
35 **WORD COUNT:** 4087

36 **ABSTRACT** (200 words)

37 Blood endothelial cells control the hemostatic and inflammatory response by secreting von  
38 Willebrand factor (VWF) and P-selectin from storage organelles called Weibel-Palade bodies  
39 (WPB). Actin-associated motor proteins regulate this secretory pathway at multiple points.  
40 Prior to fusion, myosin Va forms a complex that anchors WPBs to peripheral actin structures  
41 allowing maturation of content. Post-fusion, an actomyosin ring/coat is recruited and  
42 compresses the WPB to forcibly expel the largest VWF multimers. Here we provide the first  
43 evidence for the involvement of class I myosins during regulated VWF secretion. We show  
44 that the unconventional myosin-1C (Myo1c) is recruited post-fusion via its pleckstrin  
45 homology domain in an actin-independent process. This provides a link between the actin  
46 ring and phosphatidylinositol 4,5-bisphosphate (PIP2) at the membrane of the fused organelle  
47 and is necessary to ensure maximal VWF secretion. This is an active process requiring  
48 Myo1c ATPase activity as inhibition of class I myosins using the inhibitor

49 Pentachloropseudilin or expression of an ATPase deficient Myo1c rigor mutant perturbs the  
50 expulsion of VWF and alters the kinetics of the exocytic actin ring. These data offer a novel  
51 insight into the control of an essential physiological process and provide a new way in which  
52 it can be regulated.

### 53 **Key points**

- 54 1. Myosin-1C is utilized for actomyosin mediated expulsion of an essential blood  
55 clotting factor (von Willebrand factor).
- 56 2. Myosin-1C links the exocytic actomyosin ring to PIP2 on the plasma membrane  
57 forming anchor points that allow maximal VWF secretion.

## 58 INTRODUCTION

59 Endothelial cells (EC) contain rod-shaped storage organelles called Weibel-Palade bodies  
60 (WPB)<sup>1</sup> which owe their unique shape to their main cargo: the pro-hemostatic glycoprotein,  
61 von Willebrand factor (VWF).<sup>2</sup> VWF dimerizes in the endoplasmic reticulum and  
62 concatemerizes as it passes through the trans Golgi network (TGN) forming long parallel  
63 proteinaceous tubules that are packaged into WPB. Other cargo include the pro-inflammatory  
64 receptor P-selectin,<sup>3</sup> cytokines and agents that control tonicity; thus, exocytosis of WPB is a  
65 crucial event important during hemostasis and inflammation.<sup>4</sup>

66 Regulated secretion of VWF occurs rapidly in response to stimulation with secretagogues  
67 released during injury and inflammation.<sup>5,6</sup> Secreted VWF tubules unfurl to form strings (up  
68 to 1 mm long) anchored to the EC surface. These serve as a platform for platelet aggregation  
69 and thrombus formation.<sup>7</sup> This process instigates the primary hemostatic response but is also  
70 causally associated with thrombotic diseases such as peripheral vascular disease, myocardial  
71 infarction and stroke.<sup>8</sup> Responsible for one in four deaths,<sup>9</sup> thrombosis is a leading cause of  
72 death world-wide. While current therapy options are numerous, they are complicated by the  
73 risk of excess bleeding and cerebral hemorrhage.<sup>10</sup> As such, there remains a profound  
74 medical need for more nuanced treatment strategies.

75 Circulating levels of VWF are prognostic for cardiovascular disease<sup>11</sup> and control of  
76 regulated secretion of VWF is being actively investigated as a therapeutic strategy to reduce  
77 the burden of thrombotic diseases. Aptamers and antibodies targeting VWF are currently  
78 being tested in the clinic to limit thrombotic pathologies such as thrombotic  
79 thrombocytopenic purpura<sup>12</sup> and stroke.<sup>13</sup> We have previously identified cellular machinery  
80 that regulates the expulsion of VWF and targeting this process represents an exciting  
81 therapeutic approach. ECs recruit actin and non-muscle myosin to sites of WPB exocytosis as  
82 rings, these contract in a process aided by septins<sup>14</sup> to forcibly extrude the ultra large VWF  
83 multimers apically (into the blood vessel lumen).<sup>15</sup>

84 Myosins are molecular motor proteins that mediate organelle trafficking and contractile  
85 processes during muscle contraction, cytokinesis and protein secretion.<sup>16-18</sup> Conventional  
86 class II myosins dimerize and bind to adjacent, oppositely orientated, actin filaments via both  
87 head regions to exert force. This is known as the 'sliding filament hypothesis'.<sup>19</sup> Monomeric  
88 class I myosins are referred to as unconventional and lack these abilities. They are localized  
89 at cell membranes in ruffles, filopodia and the leading edge during migration.<sup>17</sup> Structurally,  
90 class I myosins are composed of an actin and ATP-binding head domain, a variable neck  
91 region and a tail domain.<sup>20</sup> The 'neck' (or lever) region contains calmodulin (light chain)  
92 binding IQ (isoleucine-glutamine) motif(s) which acts as a regulatory domain, similar to the  
93 light chains of class II myosins.<sup>21</sup> Lastly, class I myosins possess a pleckstrin homology (PH)  
94 domain in the tail region that facilitates binding to phosphoinositides.<sup>22</sup> In some settings,  
95 class I myosins transport intracellular vesicles along actin filaments.<sup>23,24</sup> They have also been  
96 shown to tether GLUT4-containing vesicles to actin during exocytosis.<sup>25</sup> Whereas lung  
97 surfactant secreting alveolar type II (ATII) cells utilize actin and class I myosins to aid  
98 vesicle compression during lamellar body exocytosis.<sup>26</sup>

99 A pivotal role of a subset of myosin isoforms in WPB trafficking and VWF secretion has  
100 previously been described. WPB are anchored to actin structures in the cell periphery by a  
101 tripartite complex of Rab27a, MyRIP and Myosin Va.<sup>27,28</sup> Non-muscle myosin IIA  
102 (NMIIA),<sup>29</sup> NMIIB<sup>15</sup> and Myosin Vc<sup>30</sup> have been implicated in the actomyosin mediated  
103 expulsion of VWF. However, the role of class I myosins has not been characterized.

104 We previously utilized peroxidase proteomics to identify proteins in close proximity to WPB  
105 in unstimulated and stimulated conditions.<sup>14</sup> This powerful approach identified differential  
106 proximity of actin-binding motor proteins to the WPB surface in resting ECs and in response  
107 to stimuli. Here, we describe the function of the class I myosin motor, myosin 1C (Myo1c)  
108 and suggest a crucial role in linking the contractile actin ring to the plasma membrane (PM)  
109 to augment vesicle compression.  
110

## 111 **METHODS**

### 112 **Cell culture**

113 Human Umbilical Vein ECs (HUVEC) (Cat: 12203) and Human Dermal Microvascular ECs  
114 (HDMEC) (Cat: 12212) were purchased from PromoCell. ECs were cultured as described  
115 elsewhere.<sup>31</sup> HDMEC were cultured using PromoCell Ready-to-use Growth Medium MV  
116 (Cat: 22020).

### 117 **Immunofluorescence and western blotting**

118 This was performed exactly as described elsewhere.<sup>15</sup> The commercial suppliers of antibodies  
119 used here are provided in Table S1. Confocal imaging was performed using the Zeiss LSM  
120 800 and Nikon CSU-W1 SoRa spinning disk microscope with 0.1-0.2  $\mu\text{m}$  interval Z stacks  
121 for fixed sample imaging. Where necessary image brightness and contrast was adjusted for  
122 clarity and in alignment with the American Society of Hematology Author Guidelines.

### 123 **Live cell imaging**

124 Myo1c-GFP, Myo1c-Tail+3IQ-GFP, Myo1c-K892A-GFP and Myo1c-R903A-GFP were  
125 kind gifts from Michael Ostap.<sup>22</sup> PH-PLC $\delta$ 1-GFP was a gift from Christian Halaszovich.<sup>32</sup>  
126 GFP-Myo1c was a gift from Martin Bähler (Addgene plasmid # 134832).<sup>33</sup> GFP-Myo1c  
127 (G108R) was generated in our laboratory. GFP-PIPK1 gamma 87 was a gift from Pietro De  
128 Camilli (Addgene plasmid # 22300).<sup>34</sup> GFP-VWF was a gift from J. Voorberg and J.A. Van  
129 Mourik (Sanquin Research Laboratory, Amsterdam, Netherlands).<sup>35</sup> P-Selectin luminal  
130 domain mCherry (P.sel.lum.mCherry) was previously cloned in our laboratory.<sup>15</sup> LifeAct-  
131 GFP was a gift from B. Baum (University College London, London, England, UK).<sup>36</sup>  
132 HUVEC were incubated at 37C, 5% CO<sup>2</sup> and 0.5-1  $\mu\text{m}$  interval Z stacks were obtained  
133 continuously for 5-10 minutes according to experimental objective.

### 134 **Myo1C mutagenesis**

135 Mutation of glycine 108 to arginine (G108R) changes a conserved residue of the nucleotide  
136 binding region in the motor domain and results in a rigor mutant.<sup>37 38</sup> The rigor mutant was  
137 generated as described in Edelhei et al.,<sup>39</sup> using the forward primer 5'  
138 gatttctggagagagtcgggcaggcaagaca 3' and the reverse primer 5' gtcttgctgccccgactctctccagaatc  
139 3'. Mutated residues are shown in bold, isolated clones were sequenced for verification.

### 140 **Assessment of target protein inhibition on VWF secretion using NIR fluorescent dot** 141 **blot**

142 siRNAs targeting Myo1c (Cat: L-015121-00-0005) were purchased as SMARTpools from  
143 Dharmacon (Horizon Discovery). Firefly luciferase targeted siRNA was made by Eurofins  
144 Genomics (sequence 5' cgu-acg-cgg-aau-acu-ucg 3'). Electroporation of HUVEC, VWF  
145 secretion assay and near-infrared (NIR)-fluorescent dot blot was performed as described in  
146 our previous research.<sup>14</sup> Phorbol 12-myristate 13-acetate (PMA) (100 ng/mL), thrombin (1  
147 U/mL), vascular endothelial growth factor (VEGF) (40 ng/mL), histamine (100  $\mu\text{M}$ ),  
148 adrenaline (10  $\mu\text{M}$ ) or 3-isobutyl-1-methyl xanthine (IBMX) (100  $\mu\text{M}$ ) were used to  
149 stimulate WPB exocytosis. For myosin 1 inhibition, HUVEC were exposed to  
150 Pentachloropseudilin (PCLP) (AOBIOUS, Cat: AOB33969) for 30 mins or 16 hours (5-20  
151  $\mu\text{M}$ ) prior to stimulation with secretagogue.

152 **In vivo**

153 Procedures conducted using mice were in alignment with the institutional Animal Welfare  
154 Ethical Review Body (AWERB) and UK Home Office guidelines. Eight-week-old, male,  
155 C57BL/6 mice (Charles River, UK) were housed under controlled environmental conditions  
156 (12-hour light/dark cycles at ambient temperature and humidity) on a standard chow diet.  
157 Whole-mount staining and imaging of cremasteric venules was performed as described  
158 elsewhere.<sup>40</sup>

159

## 160 RESULTS

### 161 **APEX2 proximity proteomics identified differentially enriched myosin isoforms as** 162 **putative regulators of WPB dynamics**

163 Myosin isoforms have pleiotropic functions in secretory vesicle trafficking. They are essential  
164 for pre- and post-fusion exocytic processes, including the anchoring of vesicles to peripheral  
165 actin, remodelling of cortical actin, stabilization/linking the fusion pore to the PM and force-  
166 driven compression to mediate cargo expulsion.<sup>42</sup> In order to discern which myosin isoforms  
167 were of importance in regulated VWF secretion we consulted our publicly available  
168 proximity proteomics data set.<sup>14</sup>

169 A volcano plot was generated to illustrate which myosin isoforms were most upregulated and  
170 most significantly enriched proximal to WPBs (Fig. 1A). Myosin Va (MYO5A), forms a  
171 tripartite complex with Rab27a and MYRIP in order to anchor WPBs to actin structures in  
172 the cell periphery.<sup>43</sup> As expected, Myosin Va was significantly enriched in both unstimulated  
173 and stimulated (PMA or Histamine/Adrenaline/IBMX [HAI]) Rab27a-proximity proteomic  
174 data sets.<sup>14</sup> Unexpectedly, the class IX myosin, Myosin 9B (Myo9B) was the most highly  
175 enriched and statistically significant myosin isoform proximal to WPBs in both resting and  
176 stimulated cells. This was confirmed using immunofluorescence (IF), where some Myo9B  
177 (green) could be seen proximal VWF (blue) near actin structures (magenta) and likely at focal  
178 adhesions (Fig. 1B). This unusual myosin motor has a Rho-GAP domain in its tail region.<sup>44</sup>  
179 As Rho activation has previously been implicated in VWF secretion<sup>45,46</sup> we did not anticipate  
180 that Myo9B was a positive regulator of VWF secretion. Indeed, knockdown (~82%) of  
181 Myo9B by siRNA did not affect VWF secretion following exposure to distinct secretagogues  
182 (Fig. 1C&D). Subsequently, we chose to investigate the class I myosin family, of which two  
183 isoforms were significantly enriched in proximity to WPBs (isoforms C and E) (Fig. 1A:  
184 Bold). Of these, only Myo1c was enriched exclusively following secretagogue stimulation  
185 (both PMA and HAI), indicating a potential role in regulated exocytosis. To assess the  
186 functional role of Myo1c we assessed the effect of depleting the endogenous pool of Myo1c  
187 on regulated VWF secretion. SiRNA mediated depletion resulted in knock down efficiencies  
188 of 71-88% (Fig. 1E). In agreement with a role in WPB exocytosis, Myo1c knock down  
189 reduced VWF secretion in response to PMA ( $p < 0.005$ ) (Fig. 1F). Through use of independent  
190 siRNAs against Myo1c (Fig. S1A-C) we confirmed depletion of Myo1c reduced VWF  
191 secretion in response to PMA and HAI. Furthermore, Myo1c KD reduced VWF secretion in  
192 response to the potent physiological regulators of VWF secretion VEGF165 ( $p < 0.05$ ) (Fig.  
193 1G) and thrombin ( $p < 0.01$ ) (Fig. S1D). A complicating factor is that Myo1c depletion has  
194 been reported to disrupt recycling of lipid rafts<sup>47</sup> and the trafficking of VEGFR2 to the PM  
195 resulting in lysosomal degradation.<sup>48</sup> We confirmed that endogenous VEGFR2 concentrations  
196 were significantly reduced in Myo1c KD cells ( $p < 0.01$ ) (Fig. 1H&I) as well as in HUVEC  
197 treated overnight with the pan class I myosin inhibitor, PCLP ( $p < 0.5$ ) (Fig. 1J&K). To avoid  
198 this as a confounding factor in our investigations, we hereafter used PMA as the experimental  
199 secretagogue as this chemical is a cell permeable PKC activator bypassing PM-receptor  
200 signalling.



## 201 **Myo1c is recruited during exocytosis**

202 Myo1c has proposed roles in membrane fusion of GLUT4 containing vesicles,<sup>49</sup> compression  
203 of lung surfactant secreting lamellar bodies<sup>26</sup> and for linking actin to the PM during  
204 compensatory endocytosis in frog eggs.<sup>50</sup> IF and super-resolution spinning disk microscopy  
205 of HUVEC showed that Myo1c did not co-localize with VWF in unstimulated cells (Fig. 2A:  
206 box and inset). Following secretagogue stimulation WPBs fuse with the PM and collapse as  
207 the pH of the organelle shifts from acidic to neutral<sup>4</sup> and Myo1c was apparent surrounding  
208 fused WPB. Endogenous Myo1c was localized as punctae within the actin ring but  
209 encapsulating VWF (Fig. 2A and Fig. S2A&B). Utilising the actin polymerization inhibitor,  
210 cytochalasin E (CCE) with and without stimulus, we noted that Myo1c recruitment is  
211 independent of actin (Fig. 2A). As a complementary approach, we utilized live cell imaging  
212 of HUVEC transiently expressing GFP-tagged Myo1c.<sup>33</sup> Co-expression with LifeAct-Ruby  
213 illustrated its colocalization with actin at the leading edge<sup>51</sup> (Movie S1). Whereas co-  
214 expression with P.sel.lum.mCherry<sup>15</sup> (a fusion marker which is stored in WPBs and lost upon  
215 fusion with the PM) allowed assessment of Myo1c recruitment dynamics during WPB  
216 exocytosis. In response to PMA, Myo1c-GFP was clearly recruited to WPBs post-fusion and  
217 was present on 68.65% ± 6.17 of events (Fig. 2B) (Movie S2). In agreement with this,  
218 addition of an Alexa Fluor conjugated anti-VWF antibody to the culture media during  
219 stimulation revealed that the Myo1c ring appeared before expulsion and labelling of VWF  
220 (Fig. S2C). By imaging HUVEC expressing LifeActRuby and Myo1c-GFP we noted that the  
221 Myo1c signal preceded recruitment of the actin ring (Fig. S2D).

222 To confirm our results in an alternative EC type we assessed whether human dermal  
223 microvascular ECs (HDMEC) utilized actin rings during WPB exocytosis. Live cell imaging  
224 of HDMEC expressing LifeAct-GFP and P.sel.lum.mCherry confirmed that this phenomenon  
225 is not specific to venous ECs from the umbilical vein (Fig. 2C). IF studies demonstrated that  
226 HDMEC also recruit Myo1c during VWF secretion (Fig. 2D). Once more, this was shown to  
227 be independent of actin. Through whole-mount IF imaging of the murine cremaster muscle  
228 we determined that microvascular ECs express Myo1c in vivo (Fig. S3). This demonstrates  
229 that HUVEC are a physiologically relevant model for studying Myo1c function and that  
230 Myo1c has a post-fusion role. For the remainder of the investigations, we used HUVEC as  
231 our model system.

## 232 **PIP2 mediated recruitment of Myo1c**

233 Phosphoinositides control targeted membrane traffic and are differentially distributed  
234 between cellular compartments.<sup>52</sup> Myo1c has a PIP2 binding PH domain in its tail region.<sup>22</sup>  
235 Based on research in ATII cells<sup>26</sup> we anticipated that Myo1c was potentially recruited to  
236 fusing WPBs via this region (Fig. 3A). Lipids on the organelle and PM play a variety of roles  
237 in exocytosis in diverse secretory systems.<sup>53</sup> Phosphatidic acid and PIP2 are likely important  
238 in WPB exocytosis as phospholipase D1 (PLD1) has an established role in VWF secretion.<sup>54</sup>  
239 PIP2 sensors (PH-PLC $\delta$ 1-YFP) and enzymes (PIP5K $\gamma$ 87) have previously been shown to be  
240 recruited to site of WPB fusion.<sup>55</sup> We independently confirmed that GFP-PIP5K $\gamma$ 87 (Fig. 3B)  
241 and PH-PLC $\delta$ 1-GFP (Fig. 3C) were present at sites of WPB fusion following collapse of the  
242 organelle. Interestingly, we on occasion noted the presence of GFP-positive vacuoles in GFP-  
243 PIP5K $\gamma$ 87-expressing cells that were coated in Myo1c, actin and septin 7 (another lipid  
244 binding protein associated with WPB exocytosis) (Fig. S4). These data indicate the presence  
245 of PIP2 on the PM drives protein recruitment.

246 To investigate the mechanism of its recruitment we used truncated and point mutants of  
247 Myo1c (Fig. 3D). By co-expressing the GFP-tagged neck and tail domain of Myo1c (Myo1c-  
248 Tail+3IQ-GFP) together with LifeAct-Ruby we demonstrate that the N-terminus is necessary  
249 for appropriate Myo1c targeting to actin at the leading edge (Fig. 3E and inset) (Movie S3).  
250 Consistent with the hypothesis that Myo1c is recruited to fusing WPB via its tail-resident PH  
251 domain; Myo1c-Tail+3IQ-GFP localized to fused WPBs following secretagogue stimulation  
252 (Fig. 3F). We used a GFP-tagged Myo1c fusion proteins harbouring point mutations in the  
253 phosphoinositide-binding PH domain (K892A/R903A) to show that the interaction with PIP2  
254 is necessary for recruitment to WPB at fusion (Fig. 3G&H). Unlike the wild type (WT) and  
255 Myo1c-Tail+3IQ construct; Myo1c-K892A-GFP and Myo1c-R903A-GFP localized to the  
256 cytosol and were not recruited to WPBs post-fusion. Taken together, these data indicate that  
257 Myo1c is recruited to WPB post-fusion via its PH domain.

## 258 **The effect of type I myosin inhibition on VWF secretion and exocytic actin ring** 259 **dynamics**

260 To investigate the role of the motor (head) domain we utilized the pan-myosin I inhibitor,  
261 PCLP.<sup>56</sup> PCLP is a potent allosteric inhibitor of myosin ATPase which shows selectivity for  
262 class I myosins at low doses (IC<sub>50</sub> ~ 1-10 μM). However, at higher doses, other myosin  
263 classes (e.g., NMIIB IC<sub>50</sub> ~ 90 μM)<sup>56</sup> are affected. Here, pre-exposure to 2.5-20 μM PCLP  
264 for 16 hours, resulted in an obvious trafficking defect whereby the endogenous levels of total  
265 and mature-VWF were decreased (Fig. 4A-C) (p<0.05). The ratio of pro-VWF to mature-  
266 VWF was increased in a dose-dependent fashion (Fig. 4D) (p<0.05-0.01). Regulated VWF  
267 secretion (Fig. 4E & F) and string formation (Fig. 4G-I) were almost completely abolished in  
268 PCLP treated cells. Moreover, IF of LAMP1 (Fig. 4J) and TGN46 (Fig. 4K) illustrated the  
269 appearance of VWF positive lysosomes and a gross defect in morphology of the TGN. This  
270 demonstrates that class I myosins play a role in VWF trafficking as well as secretion. To  
271 determine the specific role of Myo1c in VWF trafficking we next assessed the effect of four  
272 different siRNA oligonucleotides targeting Myo1c on VWF levels by western blotting.  
273 Quantification of the levels of mature and pro-VWF were unchanged by Myo1c knockdown  
274 indicating that Myo1c is not essential for WPB biogenesis. The broader effect of PCLP likely  
275 reflect effects on other class I myosins during WPB biogenesis (Fig. S5).

276 Short term PCLP treatment (30 minutes) allows post-fusion analysis of the role of type I  
277 myosins in WPB exocytosis by acutely inhibiting the myosin I ATPase activity without  
278 affecting WPB biogenesis (Fig. 5A). Accordingly, we first utilized PCLP to assess the effect  
279 on PMA-induced VWF secretion. Pre-incubation with 10-40 μM PCLP significantly reduced  
280 VWF secretion (p<0.05-0.01) (Fig. 5B). We next imaged HUVEC co-expressing GFP-VWF  
281 and P.sel.lum.mCherry to investigate the effect of type I myosin inhibition on VWF  
282 expulsion (Fig. 5C). PCLP significantly (p<0.01) increased the lag time for GFP-VWF to be  
283 expelled following the loss of the WPB fusion marker, P.sel.lum.mCherry (61s±9 vs 172s±13  
284 mean ± SEM) (Fig. 5D&E). To address whether this result was specific to Myo1c or a  
285 broader effect on class I myosins we repeated this loss of function assay using siRNA. We  
286 achieved KD efficiencies of ~68% (Fig. 5F). This correlated with a marked increase in the  
287 average delay between the loss of P.sel.lum.mCherry and GFP-VWF (42s±8.4 vs 99s±10.2)  
288 (Fig. 5G). Given the heterogenous nature of siRNA transfection efficiencies across a  
289 monolayer of cells we postulate the phenotype is likely an underestimation and this indicates  
290 Myo1c is the predominant class I myosin influencing WPB exocytosis.

291 Next, we studied actin dynamics during WPB exocytosis using a similar approach  
292 substituting GFP-VWF for LifeAct-GFP (Fig. 6A). This demonstrated that type I myosin  
293 inhibition with PCLP had no effect on the percentage of WPB fusion events that recruited an  
294 actin ring (Fig. 6B). This indicated that Myo1c is not required for actin polymerization.  
295 However, an increased proportion of persisting (>60s) actin coats/rings was noted in PCLP  
296 treated cells (2.4% vs 19.3%) (Fig. 6C) demonstrating that actin ring contraction required  
297 Myo1c ATP hydrolysis (Movie S4&5). This phenotype was confirmed by generating a  
298 dominant negative GFP-Myo1c rigor mutant via the introduction of a point mutation in the  
299 ATP-binding site (G108R) (Fig. 6D). Live cell imaging of GFP-Myo1c WT and GFP-Myo1c  
300 (G108R) determined that both were recruited to WPBs during exocytosis and the percentage  
301 of fusion events that were positive for Myo1c-GFP signal was comparable to that of actin  
302 rings (WT 68.7%±6.2 vs G108R 84.79%±6.1) (Fig. 6E). The WT signal persisted for

303 approximately 26 secs which also matches the dynamics of the actin ring.<sup>14,15</sup> However, the  
304 rigor mutant persisted for longer ( $\sim 57s \pm 19$ ), mirroring what we observed when imaging actin  
305 dynamics in the presence of PCLP (Fig. 6F). This was also reflected in the distribution of  
306 frequency of events. We noted a striking similarity to the change in actin ring dynamics  
307 where the percentage GFP-Myo1c rings that lasted over 60s was increased following PCLP  
308 treatment (3.8% vs 11.9%) (Fig. 6G). Using an Alexa Fluor-conjugated anti-VWF antibody  
309 in the medium we monitored VWF as it is secreted from the cell (Fig. 6H). We compared the  
310 amount of VWF secreted by the cell in relation to total VWF whilst overexpressing GFP,  
311 GFP-Myo1c WT or GFP-Myo1c (G108R). Concordant with our previous data  
312 overexpression of the “rigor” mutant resulted in reduced secretion of VWF (Fig. 6I).  
313 However, this must be caveated with potential off target effects during WPB biogenesis at the  
314 TGN (Fig. 6H arrows and Fig. S6). Taken together these data indicate a role for Myo1c and  
315 its ATPase domain in augmenting compression of the vesicle likely through actin coat  
316 organization and linkage.

## 317 DISCUSSION

318 We previously described the presence of a contractile actomyosin ring that is recruited to the  
319 WPB surface following fusion with the PM and aiding efficient VWF secretion.<sup>15</sup> This  
320 represents an unexploited therapeutic target for the prevention of thrombotic pathologies.  
321 Actomyosin mediated expulsion of VWF requires upstream protein kinase C  $\alpha$  (PKC $\alpha$ )<sup>57</sup> and  
322 p21 activated kinase 2 (PAK2)<sup>14</sup> signalling, Spire1 mediated actin nucleation,<sup>58</sup> zyxin and  $\alpha$ -  
323 actinin mediated organization<sup>59</sup> and controlled compression (via septin<sup>14</sup> and non-muscle  
324 myosin isoforms<sup>15,29</sup>). However, the mechanism by which the actomyosin ring is attached to  
325 the vesicle membrane and how this influences exocytosis is unclear. We demonstrate that  
326 Myo1c is recruited to the membrane of fused WPBs by its PH domain, in an actin-  
327 independent fashion. Perturbation of Myo1c function through pharmacological inhibition or  
328 siRNA mediated depletion reduced VWF secretion in human ECs and detailed live cell  
329 imaging experiments implicate a role in augmenting WPB exocytosis through providing  
330 additional traction points for the actin ring. This represents the first description of how class I  
331 myosin motors contribute to endothelial secretion of VWF secretion.

332 As a functional read out, we assessed the effect of siRNA mediated depletion of Myo1c on  
333 VWF secretion in response to PMA and VEGF165. These secretagogues were chosen as they  
334 stimulate increases in cytosolic cAMP and activation of PKC which is thought to be required  
335 for ring recruitment.<sup>29,57,59</sup> SiRNA depletion of Myo1c modestly reduced VWF secretion in  
336 response to PMA but a greater effect was observed when HUVEC were stimulated with  
337 VEGF165. Myo1c is known to regulate VEGFR2 trafficking to the PM and Myo1c KD leads  
338 to VEGFR2 degradation.<sup>48</sup> It is plausible that this is not specific to VEGFR2, but also other  
339 membrane bound receptors (notably we also saw a marked effect of Myo1c depletion on  
340 thrombin stimulated VWF release). For this reason, we draw our conclusions from  
341 investigations on ECs stimulated with the membrane permeable PKC agonist PMA.

342 Although other class I myosins such as Myo1e<sup>60</sup> have roles in other secretory systems, we  
343 have focused on delineating a role for Myo1c. In addition to actin-membrane tethering,  
344 Myo1c aids insulin stimulated PM-fusion of GLUT4 containing vesicles, where it is recruited  
345 prior to vesicle fusion.<sup>23,61</sup> In contrast, we observed that GFP-tagged Myo1c is recruited to  
346 the WPB surface post-fusion, similar to that reported by Kittelberger and colleagues.<sup>26</sup> We  
347 therefore exclude that Myo1c is acting as an organelle transporter. Instead, we propose a  
348 similar role to that seen in surfactant exocytosis by ATII cells<sup>26</sup> and cortical granules in  
349 *Xenopus* eggs<sup>50</sup> whereby Myo1c links the actin coat to the vesicle membrane. To fulfil this  
350 role, Myo1c requires a tight interaction with both actin and the WPB membrane surface. We  
351 show that the PH domain of Myo1c binds PIP2 that is recruited to WPB post-fusion<sup>55</sup>.  
352 Inhibition of the myosin head ATPase domain using PCLP resulted in constrained release of  
353 VWF and delayed actin ring contractility although it did not reduce the proportion of fusion  
354 events that recruited actin. We sought to confirm these findings by generating an ATP  
355 hydrolysis deficient (rigor) mutant (G108R). In the yeast homologue (Myo5), this mutation  
356 inhibits endocytosis and prevents membrane invagination.<sup>38</sup> A similar rigor mutant has also  
357 been generated by mutating a lysine 111 (K111R) that inhibits lipid raft exocytosis.<sup>47</sup> The  
358 Myo1c rigor mutant reduced the amount of VWF secreted and live cell imaging showed that  
359 it persisted at the site of fusion longer than the full-length Myo1c control. The timing of WT  
360 Myo1c recruitment mirrored the spatiotemporal dynamics of the actin ring further suggesting  
361 a role in aiding this force driven process. The change in ring kinetics following inhibition

362 with PCLP were strikingly similar to those of G108R. Overall, these changes closely  
363 resemble the defect in actin ring contraction observed when NMII isoforms are inhibited  
364 using blebbistatin<sup>15</sup> consistent with active Myo1c augmenting VWF release by providing  
365 anchor points for the actomyosin ring.

366 Here, an acute PCLP exposure time of 30 minutes was needed to assess actin ring dynamics  
367 during WPB exocytosis. Longer incubation times had drastic effects on protein trafficking.  
368 Sixteen-hour incubation with PCLP resulted in disruption of the TGN, a near complete  
369 abrogation of regulated VWF secretion, ineffective VWF biogenesis as well as the clear  
370 observation of VWF signal in LAMP1 positive lysosomes. This may reflect defects at the  
371 Golgi<sup>62</sup> or inhibition of autophagosome-lysosome fusion<sup>63</sup> with subsequent effects on WPB  
372 turnover, lysosomal co-localization and degradation of VWF. Importantly, we did not  
373 observe this phenotype in Myo1c depleted cells and therefore hypothesize that this trafficking  
374 defect is caused by inhibitory action of PCLP on other class I myosins.<sup>56</sup> Notably, Myo1b  
375 promotes the formation of tubules and carriers at remodelling TGN membranes<sup>64</sup> and has a  
376 role in secretory granule biogenesis in pancreatic Beta cells<sup>65</sup> and neuroendocrine cells.<sup>66</sup> A  
377 specific role in WPB biogenesis is therefore also a possibility.

378 Finally, as a hypothesis of the spatiotemporal recruitment of these molecules we present a  
379 putative working model (Graphical Abstract). Enriched PIP2 concentrations occur at the site  
380 of WPB fusion either as a result of membrane mixing and/or through PIPK1 $\gamma$ 87 mediated  
381 production from its precursor PI4P. PIP2 at the WPB surface then leads to the rapid  
382 recruitment of Myo1c via its lipid binding PH domain. *De novo* Spire1 mediated actin  
383 nucleation<sup>58</sup> follows (or occurs simultaneously) with the Myo1c motor domain binding to the  
384 resulting actin coat/ring. We suggest that NMII isoforms are recruited after actin, such as  
385 seen in *Xenopus* eggs<sup>67</sup>, lamellar bodies,<sup>68</sup> rodent<sup>69</sup> and *Drosophila* salivary granules.<sup>70</sup>  
386 Activation of these isoforms then leads to vesicle compression and expulsion of VWF.

387 Overall, these data provide the first evidence of class I myosins participating in VWF  
388 secretion from ECs. And to our knowledge this is the first description of a role for Myo1c in  
389 the field of thrombosis and hemostasis. As such these data aid our fundamental understanding  
390 of the molecular mechanisms governing primary hemostasis.

## 391 ACKNOWLEDGMENTS

392 The authors thank their funders and collaborators. This work was supported by the British  
393 Heart Foundation (Grant PG/22/11208). T.P.M. was funded by a Barts Charity Project Grant  
394 (MGU05434).

395 We acknowledge the CMR Advanced Bio-Imaging Facility of QMUL for the help and advice  
396 with microscopy. We thank Dr. Chris Stefan (University College London) for his critical  
397 appraisal of this manuscript.

## 398 AUTHORSHIP CONTRIBUTIONS

399 S.E.-M., and T.D.N., developed the methodology; P.M. and M.F. generated and provided  
400 essential tools and reagents; S.E.-M., T.D.N., T.P.M., T.A.J.M and G.M performed the  
401 investigation; T.D.N. supervised the study; S.E.-M. and T.D.N. wrote the original draft; and  
402 all authors reviewed and edited the manuscript.

## 403 DISCLOSURE OF CONFLICTS OF INTEREST

404 The authors declare no competing financial interests.

405 **CORRESPONDANCE**

406 Sammy El-Mansi and Thomas D. Nightingale, Centre for Microvascular Research, William  
407 Harvey Research Institute, Charterhouse Square, Faculty of Medicine and Dentistry, Queen  
408 Mary University of London, London EC1M 6BQ, United Kingdom; e-mail:  
409 s.elmansi@qmul.ac.uk and t.nightingale@qmul.ac.uk.

## 410 FIGURE LEGENDS

411 **Figure 1: WPB proximal myosin motors** (A) Volcano plot of myosin isoforms in close  
412 proximity to WPBs, previously identified by Rab27a-targeted APEX2 proximity proteomics.  
413 Blue - significantly enriched in unstimulated cells. Green – significantly enriched in PMA  
414 stimulated cells. Magenta – significantly enriched in HAI stimulated cells. Grey - not  
415 statistically significant as compared to mock transfected HUVEC. Paired *t* test. (B)  
416 Unstimulated HUVEC were fixed and subject to immunofluorescence analysis to localize  
417 Myo9B (green) in relation to VWF (blue) and actin (magenta). Myo9B staining was present  
418 in the cytoplasm and at the end of actin stress fibres reminiscent of focal adhesions. In some  
419 cases, VWF localized proximal to Myo9B puncta. Scale bar 10  $\mu$ m. Inset 1  $\mu$ m (C) Western  
420 blotting of tubulin and Myo9b in HUVEC lysate following two rounds of electroporation of  
421 300 pMoles luciferase (LUC) and Myo9B targeting siRNA. Representative blot. KD= knock  
422 down efficiency (D) VWF secretion in response to PMA, HAI and thrombin was assessed by  
423 NIR dot blot n=3. (E) Western blotting of tubulin and Myo1c in HUVEC lysate following  
424 two rounds of electroporation of 500 pM luciferase (LUC) and Myo1c targeting siRNA. (F)  
425 LUC and Myo1c KD HUVEC were exposed to PMA (100 ng/mL) or (G) VEGF165 (40  
426 ng/mL) and VWF secretion was quantified by NIR dot blot. n=3. Students *t* test. \*\*\*P<0.005  
427 \*\*P<0.01. (H) Western blotting and (I) densitometry of Myo1c, VEGFR2 and GAPDH in  
428 LUC and Myo1c KD HUVEC (n=6). (J&K) HUVEC were treated with the pan class I  
429 myosin inhibitor PCLP for 16 hours and endogenous levels of GAPDH and VEGFR2  
430 determined by western blotting. Oneway ANOVA \*P<0.05 n=3.

431 **Figure 2: Endothelial cells utilize Myo1c as part of the WPB exocytic machinery** (A)  
432 Super resolution imaging and immunofluorescent localization of endogenous Myo1c (green),  
433 actin (magenta) and VWF (blue) in unstimulated or PMA (100 ng/ml) stimulated HUVEC in  
434 the presence and absence of 1  $\mu$ M of the actin polymerization inhibitor cytochalasin E (CCE).  
435 Scale bar 10  $\mu$ m. Inset 1  $\mu$ m. Myo1c is recruited independently of actin but was dependent on  
436 stimulation with PMA. (B) Myo1c-GFP encapsulates WPB post-fusion as determined by live  
437 cell super resolution spinning disk imaging of PMA stimulated (100 ng/mL) HUVEC co-  
438 expressing a Myo1c-GFP and the WPB fusion marker P.sel.lum.mCherry. Scale bar 1  $\mu$ m.  
439 Arrow indicates point of collapse/fusion of vesicle (C) Live cell imaging of LifeAct-GFP and  
440 P.sel.lum.mCherry expressing HDMEC indicated the utility of actin rings to expel VWF  
441 following stimulation. Scale bar 10  $\mu$ m. Inset 1  $\mu$ m. 0.5  $\mu$ m Z stacks were acquired  
442 continuously for 10 minutes (Zeiss LSM 800) (D) Confocal imaging and IF analyses of  
443 endogenous Myo1c in HDMEC that were left untreated or stimulated with PMA, CCE or  
444 CCE and PMA. White arrows illustrate where Myo1c is recruited to fused/collapsed WPB.  
445 Scale bar 10  $\mu$ m.

446 **Figure 3: The PH domain of Myo1c is required for its recruitment during WPB**  
447 **exocytosis.** (A) A schematic of the proposed spatiotemporal dynamics of Myo1c recruitment  
448 during WPB exocytosis. (B) Live cell imaging of the GFP-PIP2K1 $\gamma$ 87 and P.sel.lum.mCherry  
449 in secretagogue (HAI) stimulated HUVEC illustrates post-fusion recruitment. Two exocytic  
450 events are seen here. Scale bars are 1  $\mu$ m. White and magenta arrows indicate independent  
451 fusion events. (C) The PIP2 sensor PH-PLC $\delta$ 1-GFP is also recruited post fusion. Scale bars  
452 are 1  $\mu$ m (D) A schematic of the Myo1c structural domains and location of truncation or site  
453 directed mutations. (E) HUVEC co-expressing LifeAct-Ruby and Myo1c-Tail+3IQ-GFP  
454 indicated the importance of the myosin head domain for interacting with actin. Scale bars are



455 10  $\mu\text{m}$  (F) Myo1c-Tail+3IQ-GFP is recruited to WPBs post-fusion (G&H) GFP-tagged  
456 Myo1c fusion proteins harbouring mutations in their PH domain (K892A/R903A) are not  
457 recruited to WPBs during exocytosis. F, G & H Scale bars are 10  $\mu\text{m}$ . Inset scale bars are 1  
458  $\mu\text{m}$ . For live cell confocal imaging experiments 0.5  $\mu\text{m}$  Z stacks were acquired continuously  
459 for 5-10 minutes (Zeiss LSM 800).

460 **Figure 4: HUVEC exposed to PCLP for 16 hours exhibit a VWF trafficking defect.**

461 HUVEC were exposed to DMSO or a range of concentrations of PCLP and incubated  
462 overnight (16 hours). (A) Immunoblotting of the resulting lysates displayed changes in pro-  
463 and mature-VWF in relation to tubulin. Densitometry indicated a decrease in (B) total VWF  
464 and (C) mature-VWF levels alongside a dose-dependent increase in the (D) ratio of  
465 pro/mature VWF.  $n=4$  Ratio paired  $t$  test. \* $P<0.05$  \*\* $P<0.01$  \*\*\*  $P<0.005$  (E) 16-hour  
466 incubation with PCLP resulted in inhibition of regulated secretion of VWF in response to  
467 thrombin and (F) HAI. (G) HUVEC pre-incubated with DMSO or PCLP for 16 hours were  
468 stimulated with HAI for 10 minutes before application of 5  $\text{dyne}/\text{cm}^2$  shear stress. VWF  
469 strings were visualized by immunofluorescence and confocal microscopy. (H) The number  
470 and (I) length of VWF strings secreted under flow in response to HAI in the presence or  
471 absence of DMSO or PCLP ( $n=3$ ). (J) IF analyses using anti-LAMP1 (green) and anti-VWF  
472 (blue) antibodies indicated numerous VWF positive lysosomes in PCLP treated cells. (K) IF  
473 analyses using anti-TGN46 (yellow) and anti-VWF (blue) antibodies indicated a gross defect  
474 in TGN morphology (fragmented and swollen) in PCLP treated cells. Scale bars 10  $\mu\text{m}$ . Inset  
475 scale bars 1  $\mu\text{m}$ .

476 **Figure 5: Acute inhibition of class I myosins and Myo1c depletion perturbs the**

477 **expulsion of VWF**(A) Schematic of Myo1c domains and mechanism of inhibition by PCLP.  
478 (B) Pharmacological inhibition of the ATP binding domain with 10-40  $\mu\text{M}$  PCLP reduces  
479 VWF release. ( $n=6$ ) \* $P<0.05$ , \*\* $P<0.01$  ratio paired  $t$  test. (C) Schematic of live cell  
480 imaging approach to study WPB fusion dynamics and VWF expulsion. Scale bar 1  $\mu\text{m}$ . (D)  
481 HUVEC were electroporated with the P.sel.lum.mCherry and GFP-VWF constructs and  
482 imaged by confocal microscopy. Preincubation with 20  $\mu\text{M}$  PCLP increased the time taken  
483 for VWF to be expelled following loss of the fusion marker (P.sel.lum.mCherry). Students  $t$   
484 test \*\* $P<0.01$ . [ $n=3$  DMSO: 9 cells, 63 events PCLP: 9 cells, 38 events Mean  $\pm$  SEM]. (E)A  
485 frequency distribution of events. (F) LUC and Myo1c KD HUVEC were used to test whether  
486 these effects were specific to Myo1c or a broader effect of class I myosins. Western blotting  
487 determined the efficiency of target protein knockdown. (G) Myo1c siRNA depletion  
488 increased the time taken for VWF to be expelled following loss of P.sel.lum.mCherry.  
489 Students  $t$  test \* $P<0.05$ .

490 **Figure 6: Inhibition of Myo1 ATPase activity through pharmacological inhibition or**

491 **point mutation (G108R) effects the actomyosin machinery associated with exocytosis.**  
492 (A) Schematic of live cell imaging approach to study actin dynamics during WPB exocytosis.  
493 Scale bar 1  $\mu\text{m}$ . (B) PMA stimulated HUVEC co-expressing LifeAct-GFP and  
494 P.sel.lum.mCherry in the presence or absence of PCLP. The percentage of WPB fusion  
495 events that recruited an actin ring were unchanged in DMSO and PCLP (20  $\mu\text{M}$ ) treated cells.  
496 (C) The lifetime (secs) of LifeAct-GFP signal at fusion sites was quantified in DMSO and  
497 PCLP treated HUVEC. The distribution of frequency of events is presented here [ $n=5$   
498 DMSO: 15 cells, 81 events PCLP: 18 cells, 93 events Mean  $\pm$  SEM] (D) Schematic of site-  
499 directed mutagenesis for the generation of a Myo1c rigor mutant. (E) HUVEC co-expressing

500 GFP tagged Myo1c constructs and P.sel.lum.mCherry were stimulated with PMA and the  
501 percentage of exocytic events that recruit GFP-Myo1c WT or G108R was quantified (n=3  
502 WT: 8 cells, 119 events G108R: 8 cells, 58 events) (F) HUVEC co-expressing GFP tagged  
503 Myo1c constructs and P.sel.lum.mCherry were stimulated with PMA and the duration of GFP  
504 signal in a ring shape forming at the site of WPB fusion was quantified. (n=3 WT: 9 cells, 79  
505 events PCLP 9 cells, 42 events). (G) The distribution of frequency closely resembles actin  
506 ring dynamics - panel C. For live cell confocal imaging experiments 0.5  $\mu\text{m}$  Z stacks were  
507 acquired continuously for 5-10 minutes (Zeiss LSM 800). (H) HUVEC expressing GFP,  
508 GFP-Myo1c (WT) or (G108R) were stimulated with PMA (100 ng/ml) for 10 min and  
509 labelled for external VWF (red) and total VWF (blue). Scale bar 1  $\mu\text{m}$ . (I) Quantification of  
510 the ratio of externalized VWF to total VWF. \*P<0.05 One way ANOVA. N=3 NTC= non-  
511 transfected control. Arrows indicate swollen intracellular VWF signal in cells expressing the  
512 G108R point mutant.

513 **Graphical abstract: A working model for actomyosin mediated expulsion of VWF.**

514 Under resting conditions WPB are anchored to peripheral actin structure via  
515 Rab27a/MyRIP/MyoVa. (1) Following stimulation WPB are trafficked to the plasma  
516 membrane where they will fuse. (2) An enrichment of PIP2 is present at the site of fusion,  
517 possibly also on the WPB surface. This could be through membrane mixing or through the  
518 catalytic activity of PIPK1 $\gamma$ 87. (3) Myo1c is recruited to the WPB via its PIP2 binding PH  
519 domain. (4) Spire1 mediated *de novo* actin nucleation could either occur after Myo1c  
520 recruitment or simultaneously. (5) Recruitment of NMII isoforms likely happens after actin  
521 polymerization. Activation of NMII allows for the expulsion of VWF into the blood vessel  
522 lumen.

## 523 REFERENCES

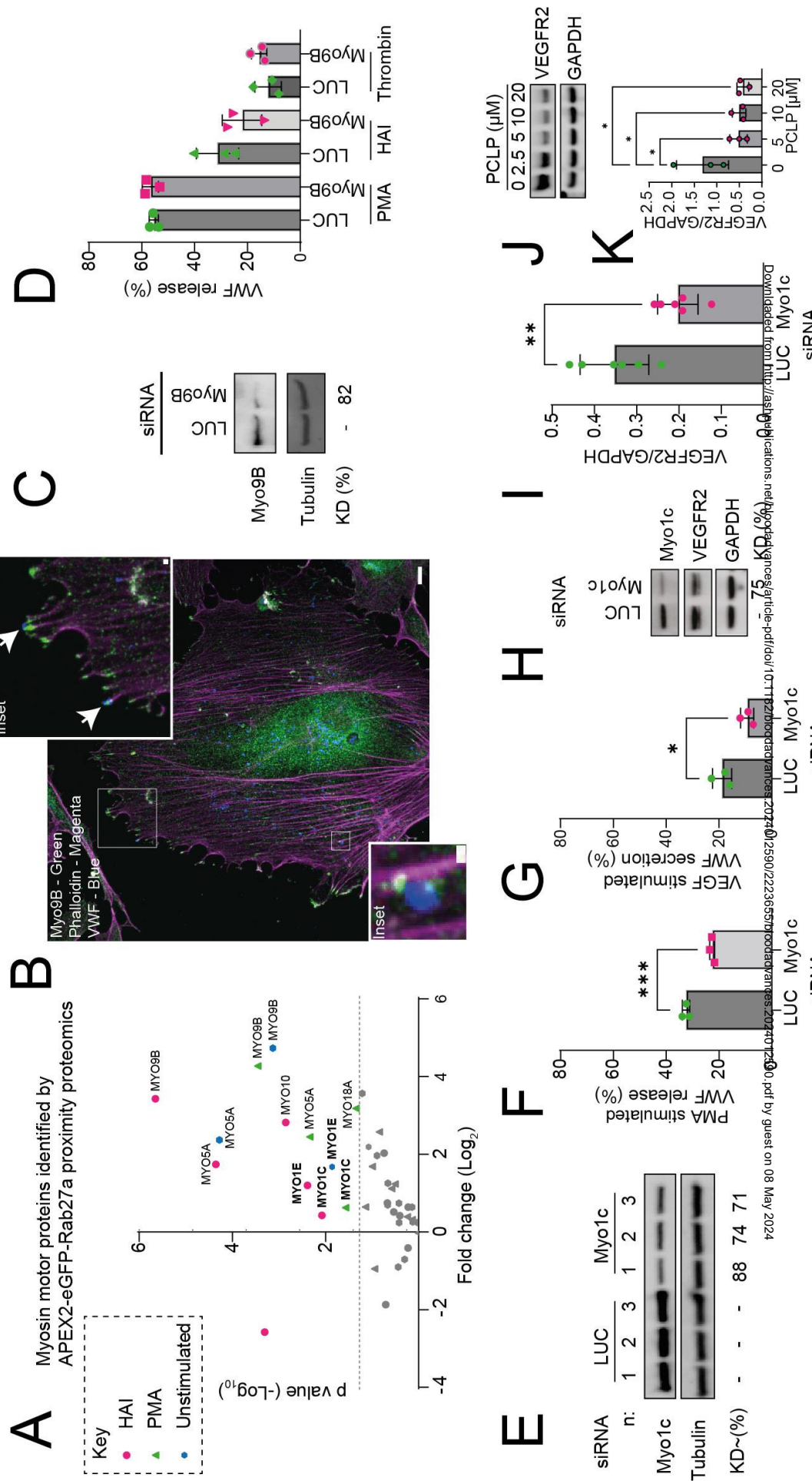
- 524 1. Weibel ER, Palade GE. New cytoplasmic components in arterial endothelia *J Cell Biol.* 1964;23:101-112.  
525
- 526 2. Wagner DD, Olmsted JB, Marder VJ. Immunolocalization of von Willebrand protein in  
527 Weibel-Palade bodies of human endothelial cells. *J Cell Biol.* 1982;95(1):355-360.
- 528 3. Larsen E, Celi A, Gilbert GE, et al. PADGEM protein: a receptor that mediates the interaction  
529 of activated platelets with neutrophils and monocytes. *Cell.* 1989;59(2):305-312.
- 530 4. McCormack JJ, Lopes da Silva M, Ferraro F, Patella F, Cutler DF. Weibel-Palade bodies at a  
531 glance. *Journal of Cell Science.* 2017;130(21):3611-3617.
- 532 5. Tsai HM, Nagel RL, Hatcher VB, Seaton AC, Sussman, II. The high molecular weight form of  
533 endothelial cell von Willebrand factor is released by the regulated pathway. *Br J Haematol.*  
534 1991;79(2):239-245.
- 535 6. Sporn LA, Marder VJ, Wagner DD. Inducible secretion of large, biologically potent von  
536 Willebrand factor multimers. *Cell.* 1986;46(2):185-190.
- 537 7. Dong JF, Moake JL, Nolasco L, et al. ADAMTS-13 rapidly cleaves newly secreted ultralarge  
538 von Willebrand factor multimers on the endothelial surface under flowing conditions. *Blood.*  
539 2002;100(12):4033-4039.
- 540 8. Manz XD, Bogaard HJ, Aman J. Regulation of VWF (Von Willebrand Factor) in Inflammatory  
541 Thrombosis. *Arteriosclerosis, Thrombosis, and Vascular Biology.* 2022;42(11):1307-1320.
- 542 9. Wendelboe AM, Raskob GE. Global Burden of Thrombosis: Epidemiologic Aspects. *Circ Res.*  
543 2016;118(9):1340-1347.
- 544 10. Mackman N, Bergmeier W, Stouffer GA, Weitz JI. Therapeutic strategies for thrombosis: new  
545 targets and approaches. *Nature Reviews Drug Discovery.* 2020;19(5):333-352.
- 546 11. Spiel AO, Gilbert JC, Jilma B. Von Willebrand Factor in Cardiovascular Disease. *Circulation.*  
547 2008;117(11):1449-1459.
- 548 12. El-Mansi S, Nightingale TD. Emerging mechanisms to modulate VWF release from  
549 endothelial cells. *The International Journal of Biochemistry & Cell Biology.* 2021;131:105900.
- 550 13. Schutgens REG. Aptamers Targeting Von Willebrand Factor: What and Why? *HemaSphere.*  
551 2023;7(2):e830.
- 552 14. El-Mansi S, Robinson CL, Kostelnik KB, et al. Proximity proteomics identifies septin and PAK2  
553 as decisive regulators of actomyosin expulsion of von Willebrand factor. *Blood.* 2022.
- 554 15. Nightingale TD, White IJ, Doyle EL, et al. Actomyosin II contractility expels von Willebrand  
555 factor from Weibel-Palade bodies during exocytosis. *J Cell Biol.* 2011;194(4):613-629.
- 556 16. Quintanilla MA, Hammer JA, Beach JR. Non-muscle myosin 2 at a glance. *Journal of Cell*  
557 *Science.* 2023;136(5).
- 558 17. McIntosh BB, Ostap EM. Myosin-I molecular motors at a glance. *J Cell Sci.*  
559 2016;129(14):2689-2695.
- 560 18. Hartman MA, Spudich JA. The myosin superfamily at a glance. *J Cell Sci.* 2012;125(Pt 7):1627-  
561 1632.
- 562 19. Woolner S, Bement WM. Unconventional myosins acting unconventionally. *Trends Cell Biol.*  
563 2009;19(6):245-252.
- 564 20. Barylko B, Jung G, Albanesi JP. Structure, function, and regulation of myosin 1C. *Acta*  
565 *Biochim Pol.* 2005;52(2):373-380.
- 566 21. Zhu T, Beckingham K, Ikebe M. High affinity Ca<sup>2+</sup> binding sites of calmodulin are critical for  
567 the regulation of myosin Ibeta motor function. *J Biol Chem.* 1998;273(32):20481-20486.
- 568 22. Hokanson DE, Laakso JM, Lin T, Sept D, Ostap EM. Myo1c binds phosphoinositides through a  
569 putative pleckstrin homology domain. *Mol Biol Cell.* 2006;17(11):4856-4865.
- 570 23. Bose A, Guilherme A, Robida SI, et al. Glucose transporter recycling in response to insulin is  
571 facilitated by myosin Myo1c. *Nature.* 2002;420(6917):821-824.

- 572 24. Cordonnier MN, Dauzonne D, Louvard D, Coudrier E. Actin filaments and myosin I alpha  
573 cooperate with microtubules for the movement of lysosomes. *Mol Biol Cell*.  
574 2001;12(12):4013-4029.
- 575 25. Boguslavsky S, Chiu T, Foley KP, et al. Myo1c binding to submembrane actin mediates  
576 insulin-induced tethering of GLUT4 vesicles. *Mol Biol Cell*. 2012;23(20):4065-4078.
- 577 26. Kittelberger N, Breunig M, Martin R, Knölker H-J, Miklavc P. The role of myosin 1c and  
578 myosin 1b in surfactant exocytosis. *Journal of cell science*. 2016;129(8):1685-1696.
- 579 27. Conte IL, Hellen N, Bierings R, et al. Interaction between MyRIP and the actin cytoskeleton  
580 regulates Weibel–Palade body trafficking and exocytosis. 2016;129(3):592-603.
- 581 28. Nightingale TD, Pattni K, Hume AN, Seabra MC, Cutler DF. Rab27a and MyRIP regulate the  
582 amount and multimeric state of VWF released from endothelial cells. *Blood*.  
583 2009;113(20):5010-5018.
- 584 29. Li P, Wei G, Cao Y, et al. Myosin IIa is critical for cAMP-mediated endothelial secretion of von  
585 Willebrand factor. *Blood*. 2018;131(6):686-698.
- 586 30. Holthenrich A, Terplane J, Naß J, Mietkowska M, Kerkhoff E, Gerke V. Spire1 and Myosin Vc  
587 promote Ca<sup>2+</sup>-evoked externalization of von Willebrand factor in endothelial cells. *Cellular  
588 and Molecular Life Sciences*. 2022;79(2):96.
- 589 31. Michaux G, Abbitt KB, Collinson LM, Haberichter SL, Norman KE, Cutler DF. The physiological  
590 function of von Willebrand's factor depends on its tubular storage in endothelial Weibel-  
591 Palade bodies. *Dev Cell*. 2006;10(2):223-232.
- 592 32. Halaszovich CR, Leitner MG, Mavrantoni A, et al. A human phospholipid phosphatase  
593 activated by a transmembrane control module. *Journal of Lipid Research*. 2012;53(11):2266-  
594 2274.
- 595 33. Ruppert C, Godel J, Müller RT, Kroschewski R, Reinhard J, Bähler M. Localization of the rat  
596 myosin I molecules myr 1 and myr 2 and in vivo targeting of their tail domains. *J Cell Sci*.  
597 1995;108 ( Pt 12):3775-3786.
- 598 34. Di Paolo G, Pellegrini L, Letinic K, et al. Recruitment and regulation of phosphatidylinositol  
599 phosphate kinase type 1 gamma by the FERM domain of talin. *Nature*. 2002;420(6911):85-  
600 89.
- 601 35. Romani de Wit T, Rondaij MG, Hordijk PL, Voorberg J, van Mourik JA. Real-time imaging of  
602 the dynamics and secretory behavior of Weibel-Palade bodies. *Arterioscler Thromb Vasc  
603 Biol*. 2003;23(5):755-761.
- 604 36. Riedl J, Crevenna AH, Kessenbrock K, et al. Lifeact: a versatile marker to visualize F-actin. *Nat  
605 Methods*. 2008;5(7):605-607.
- 606 37. Sun Y, Martin AC, Drubin DG. Endocytic internalization in budding yeast requires coordinated  
607 actin nucleation and myosin motor activity. *Dev Cell*. 2006;11(1):33-46.
- 608 38. Manenschijn HE, Picco A, Mund M, Rivier-Cordey A-S, Ries J, Kaksonen M. Type-I myosins  
609 promote actin polymerization to drive membrane bending in endocytosis. *eLife*.  
610 2019;8:e44215.
- 611 39. Edelheit O, Hanukoglu A, Hanukoglu I. Simple and efficient site-directed mutagenesis using  
612 two single-primer reactions in parallel to generate mutants for protein structure-function  
613 studies. *BMC Biotechnology*. 2009;9(1):61.
- 614 40. Owen-Woods C, Joulia R, Barkaway A, et al. Local microvascular leakage promotes trafficking  
615 of activated neutrophils to remote organs. *J Clin Invest*. 2020;130(5):2301-2318.
- 616 41. Perez-Riverol Y, Bai J, Bandla C, et al. The PRIDE database resources in 2022: a hub for mass  
617 spectrometry-based proteomics evidences. *Nucleic Acids Res*. 2022;50(D1):D543-d552.
- 618 42. Miklavc P, Frick M. Actin and Myosin in Non-Neuronal Exocytosis. *Cells*. 2020;9(6).
- 619 43. Rojo Pulido I, Nightingale TD, Darchen F, Seabra MC, Cutler DF, Gerke V. Myosin Va acts in  
620 concert with Rab27a and MyRIP to regulate acute von-Willebrand factor release from  
621 endothelial cells. *Traffic*. 2011;12(10):1371-1382.

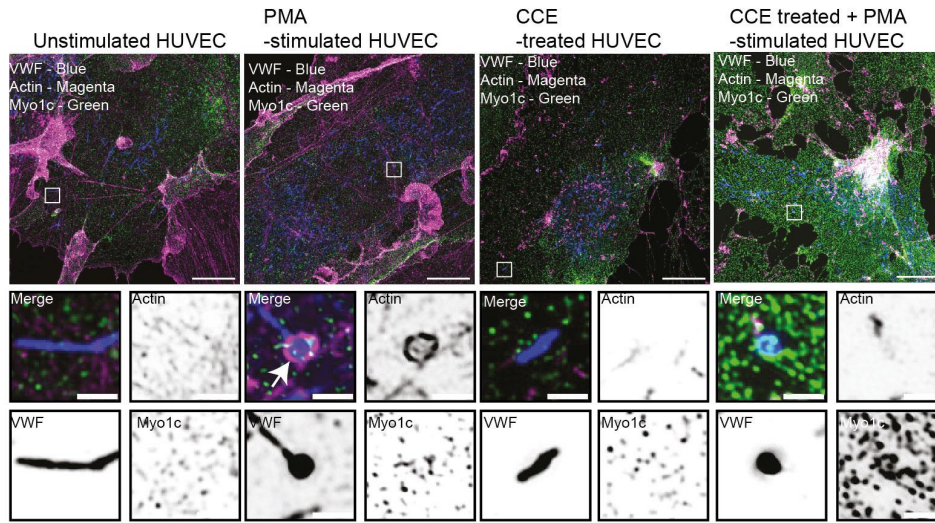
- 622 44. Hanley PJ, Xu Y, Kronlage M, et al. Motorized RhoGAP myosin IXb (Myo9b) controls cell  
623 shape and motility. *Proceedings of the National Academy of Sciences*. 2010;107(27):12145-  
624 12150.
- 625 45. Rusu L, Andreeva A, Visintine DJ, et al. G protein-dependent basal and evoked endothelial  
626 cell vWF secretion. *Blood*. 2014;123(3):442-450.
- 627 46. Mietkowska M, Schuberth C, Wedlich-Soldner R, Gerke V. Actin dynamics during Ca<sup>2+</sup>-  
628 dependent exocytosis of endothelial Weibel-Palade bodies. *Biochim Biophys Acta Mol Cell*  
629 *Res*. 2019;1866(7):1218-1229.
- 630 47. Brandstaetter H, Kendrick-Jones J, Buss F. Myo1c regulates lipid raft recycling to control cell  
631 spreading, migration and Salmonella invasion. *Journal of Cell Science*. 2012;125(8):1991-  
632 2003.
- 633 48. Tiwari A, Jung JJ, Inamdar SM, Nihalani D, Choudhury A. The myosin motor Myo1c is  
634 required for VEGFR2 delivery to the cell surface and for angiogenic signaling. *Am J Physiol*  
635 *Heart Circ Physiol*. 2013;304(5):H687-696.
- 636 49. Bose A, Robida S, Furcinitti PS, et al. Unconventional Myosin Myo1c Promotes Membrane  
637 Fusion in a Regulated Exocytic Pathway. *Molecular and Cellular Biology*. 2004;24(12):5447-  
638 5458.
- 639 50. Sokac AM, Schietroma C, Gundersen Cameron B, Bement WM. Myosin-1c Couples  
640 Assembling Actin to Membranes to Drive Compensatory Endocytosis. *Developmental Cell*.  
641 2006;11(5):629-640.
- 642 51. Fan Y, Eswarappa SM, Hitomi M, Fox PL. Myo1c facilitates G-actin transport to the leading  
643 edge of migrating endothelial cells. *J Cell Biol*. 2012;198(1):47-55.
- 644 52. Posor Y, Jang W, Haucke V. Phosphoinositides as membrane organizers. *Nature Reviews*  
645 *Molecular Cell Biology*. 2022;23(12):797-816.
- 646 53. Ammar M, Kassas N, Chasserot-Golaz S, Bader M-F, Vitale N. Lipids in Regulated Exocytosis:  
647 What are They Doing? *Frontiers in Endocrinology*. 2013;4.
- 648 54. Disse J, Vitale N, Bader MF, Gerke V. Phospholipase D1 is specifically required for regulated  
649 secretion of von Willebrand factor from endothelial cells. *Blood*. 2009;113(4):973-980.
- 650 55. Nguyen TTN, Koerdt SN, Gerke V. Plasma membrane phosphatidylinositol (4,5)-bisphosphate  
651 promotes Weibel-Palade body exocytosis. *Life Sci Alliance*. 2020;3(11).
- 652 56. Chinthalapudi K, Taft MH, Martin R, et al. Mechanism and specificity of  
653 pentachloropseudilin-mediated inhibition of myosin motor activity. *J Biol Chem*.  
654 2011;286(34):29700-29708.
- 655 57. Nightingale TD, McCormack JJ, Grimes W, et al. Tuning the endothelial response: differential  
656 release of exocytic cargos from Weibel-Palade bodies. *J Thromb Haemost*. 2018;16(9):1873-  
657 1886.
- 658 58. Holthenrich A, Terglane J, Naß J, Mietkowska M, Kerkhoff E, Gerke V. Spire1 and Myosin Vc  
659 promote Ca<sup>2+</sup>-evoked externalization of von Willebrand factor in endothelial cells. *Cell Mol*  
660 *Life Sci*. 2022;79(2):96.
- 661 59. Han X, Li P, Yang Z, et al. Zyxin regulates endothelial von Willebrand factor secretion by  
662 reorganizing actin filaments around exocytic granules. *Nature Communications*.  
663 2017;8(1):14639.
- 664 60. Schietroma C, Yu HY, Wagner MC, Umbach JA, Bement WM, Gundersen CB. A role for  
665 myosin 1e in cortical granule exocytosis in *Xenopus* oocytes. *J Biol Chem*.  
666 2007;282(40):29504-29513.
- 667 61. Toyoda T, An D, Witczak CA, et al. Myo1c Regulates Glucose Uptake in Mouse Skeletal  
668 Muscle <sup>\*</sup>. *Journal of Biological Chemistry*. 2011;286(6):4133-4140.
- 669 62. Capmany A, Yoshimura A, Kerdous R, et al. MYO1C stabilizes actin and facilitates the arrival  
670 of transport carriers at the Golgi complex. *J Cell Sci*. 2019;132(8).

- 671 63. Brandstaetter H, Kishi-Itakura C, Tumbarello DA, Manstein DJ, Buss F. Loss of functional  
672 MYO1C/myosin 1c, a motor protein involved in lipid raft trafficking, disrupts  
673 autophagosome-lysosome fusion. *Autophagy*. 2014;10(12):2310-2323.
- 674 64. Almeida CG, Yamada A, Tenza D, Louvard D, Raposo G, Coudrier E. Myosin 1b promotes the  
675 formation of post-Golgi carriers by regulating actin assembly and membrane remodelling at  
676 the trans-Golgi network. *Nat Cell Biol*. 2011;13(7):779-789.
- 677 65. Tokuo H, Komaba S, Coluccio LM. In pancreatic  $\beta$ -cells myosin 1b regulates glucose-  
678 stimulated insulin secretion by modulating an early step in insulin granule trafficking from  
679 the Golgi. *Mol Biol Cell*. 2021;32(12):1210-1220.
- 680 66. Delestre-Delacour C, Carmon O, Laguerre F, et al. Myosin 1b and F-actin are involved in the  
681 control of secretory granule biogenesis. *Scientific Reports*. 2017;7(1):5172.
- 682 67. Yu HY, Bement WM. Multiple myosins are required to coordinate actin assembly with coat  
683 compression during compensatory endocytosis. *Mol Biol Cell*. 2007;18(10):4096-4105.
- 684 68. Miklavc P, Ehinger K, Sultan A, et al. Actin depolymerisation and crosslinking join forces with  
685 myosin II to contract actin coats on fused secretory vesicles. *Journal of Cell Science*.  
686 2015;128(6):1193-1203.
- 687 69. Milberg O, Shitara A, Ebrahim S, et al. Concerted actions of distinct nonmuscle myosin II  
688 isoforms drive intracellular membrane remodeling in live animals. *J Cell Biol*.  
689 2017;216(7):1925-1936.
- 690 70. Tran DT, Masedunskas A, Weigert R, Ten Hagen KG. Arp2/3-mediated F-actin formation  
691 controls regulated exocytosis in vivo. *Nature Communications*. 2015;6(1):10098.
- 692

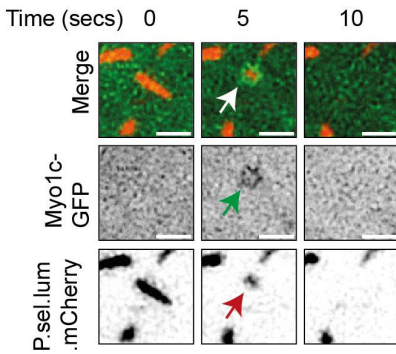
Figure 1 Figure 1



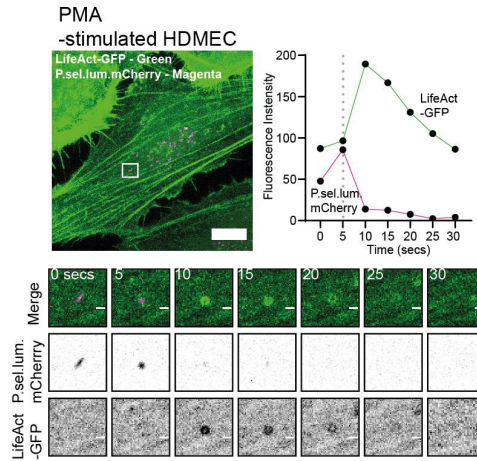
**A**



**B**



**C**



**D**

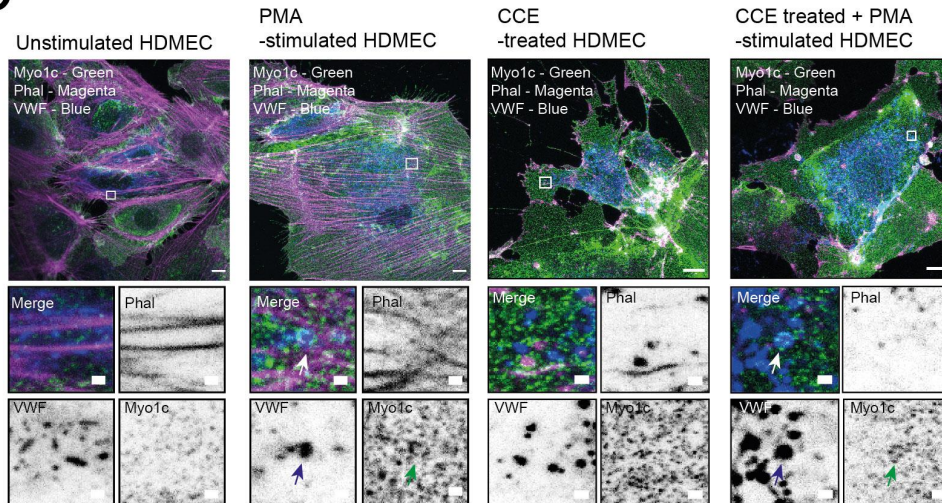




# Figure 3

Figure 3

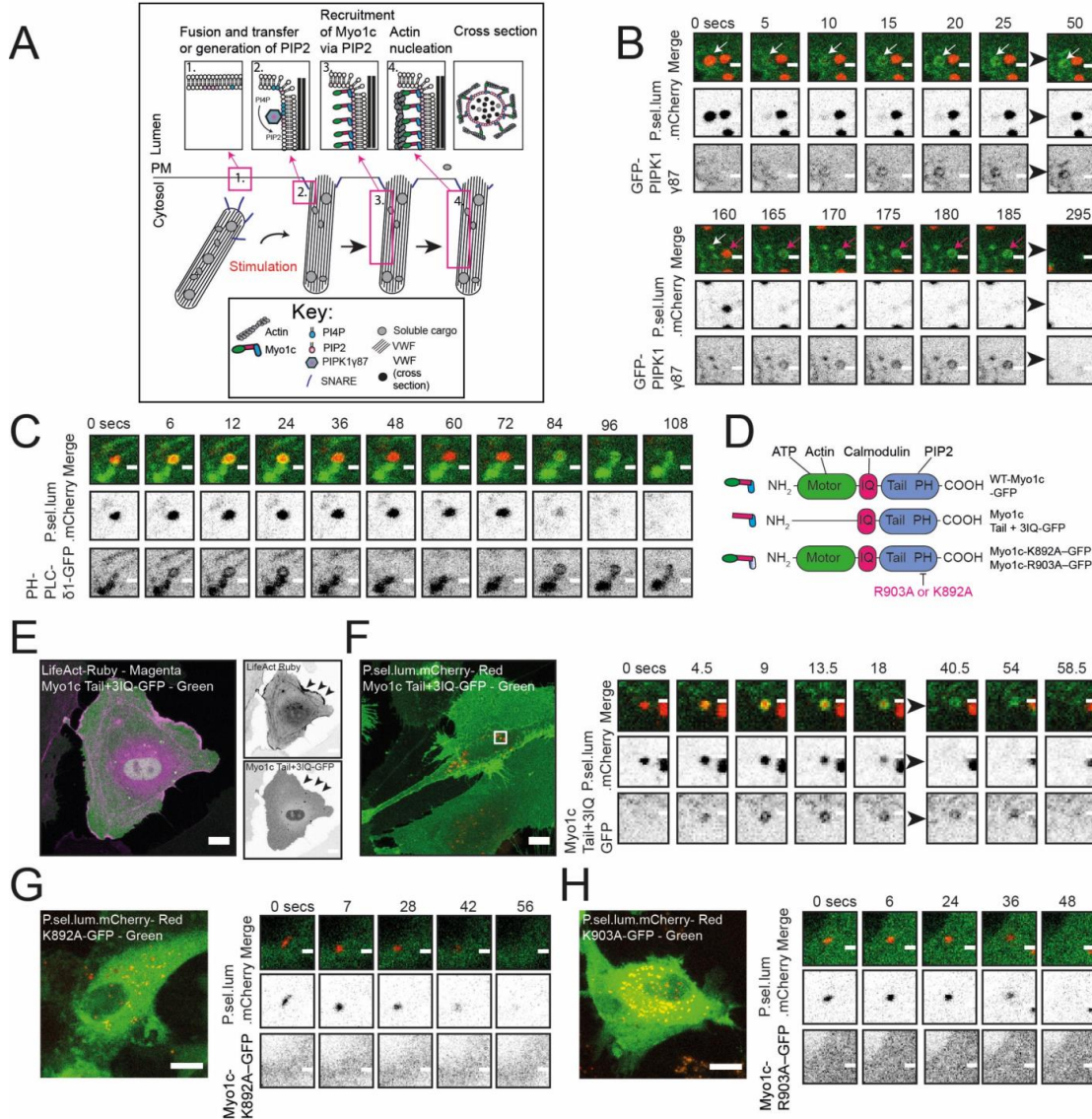
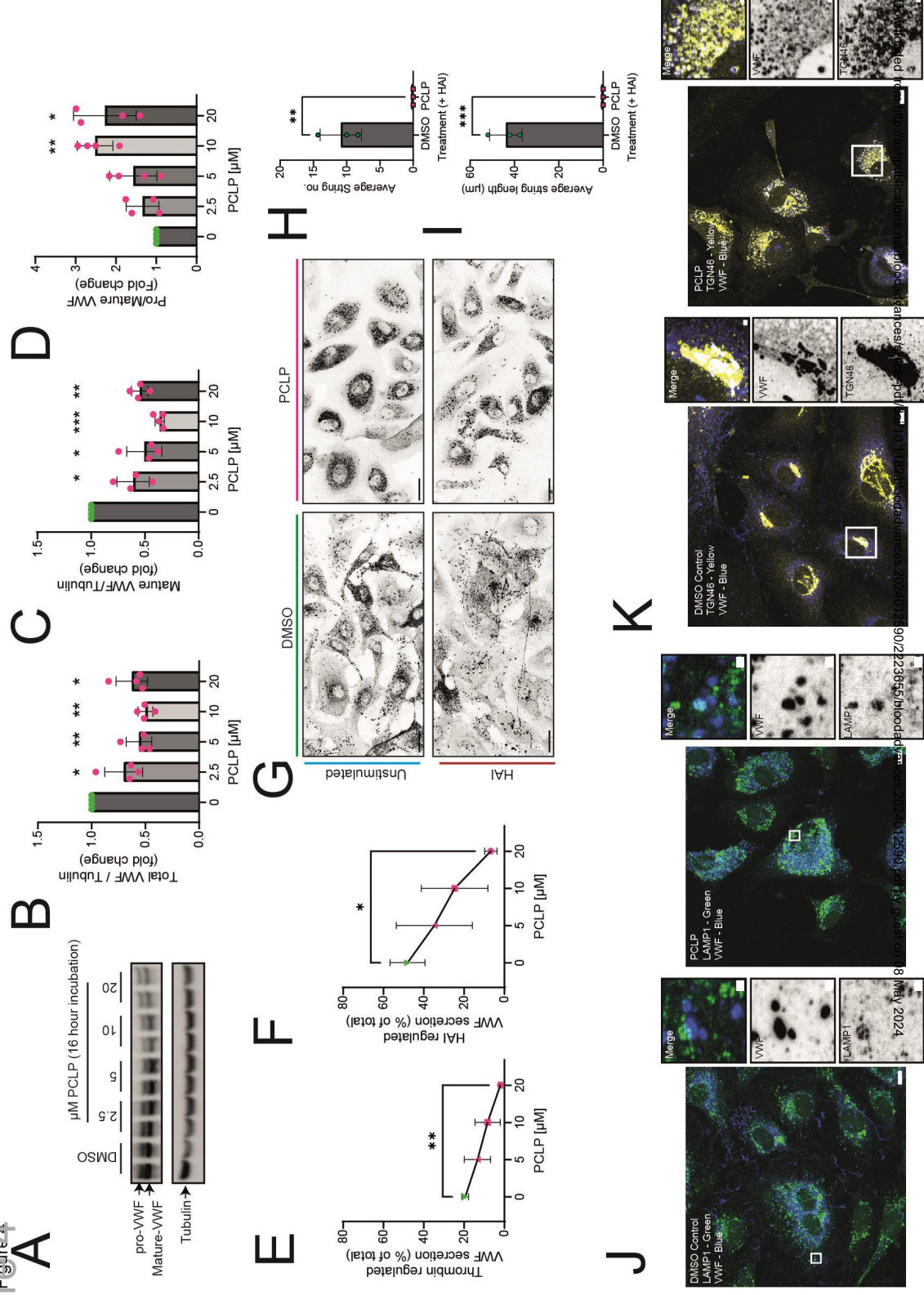


Figure 4



bioRxiv preprint doi: <https://doi.org/10.1101/2024.05.15.598188>; this version posted May 18, 2024. The copyright holder for this preprint (which was not certified by peer review) is the author/funder, who has granted bioRxiv a license to display the preprint in perpetuity. It is made available under aCC-BY 4.0 International license.

Figure 5

Figure 5

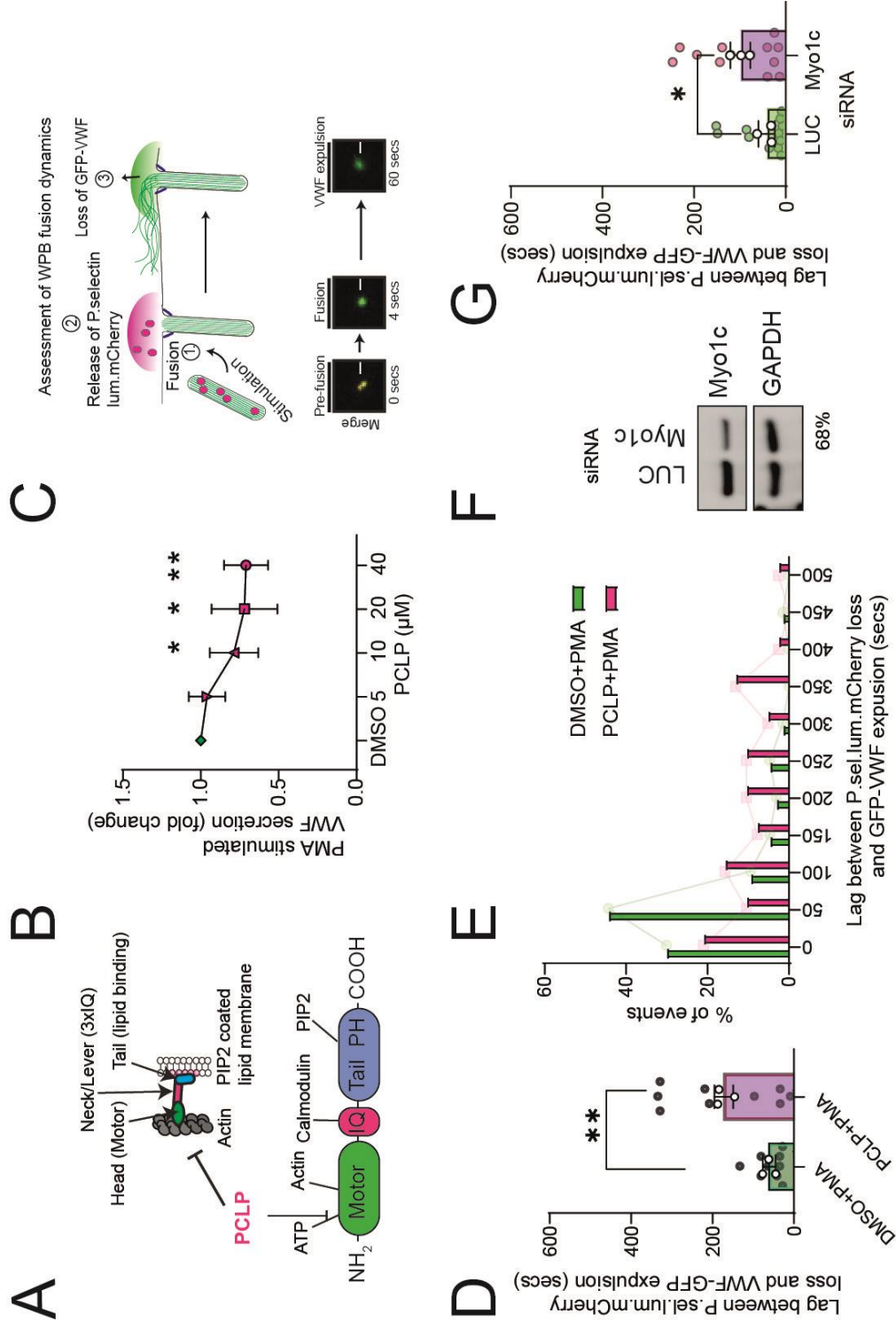


Figure 6

